Levinger et al., 2009 Supplementary Figure 1

Wild type *D. melanogaster* tRNase Z has a MW_{App} of ~90 kD (Supplementary Figure 1A; 32); as predicted for a 42 residue deletion, ΔFA183/226 displays a MW_{App} ~5 kD lower than that of WT tRNase Z. The pre-tRNA substrate (Supplementary Figure 1B), a canonical tRNA with a 17 nt 3' end trailer, was previously used to analyze tRNase Z processing kinetics (17). Based on results of efficiency experiments (data not shown), a concentration of ΔFA tRNase Z ~100-fold higher than wild type enzyme (WT: 63 pM; ΔFA: 6.6 nM; Supplementary Figure 1C, D) was used for kinetic analysis. The substrate concentration range was higher for ΔFA (WT: 5 – 125 nM; ΔFA: 250 – 6250 nM in this experiment) based on repeated kinetic experiments which showed the K_M for ΔFA tRNase Z to be ~100-fold higher than that for WT tRNase Z. The percentage of product obtained in a reaction time course (5-10-15 min. at 28 C) decreases with increasing unlabeled substrate concentration (Supplementary Figure 1C) as expected; % Prod/min is equivalent to V/[S]. Experimental data and the [S] values combine for the determination of V_{max} and K_M (from nonlinear regression analysis of the Michaelis-Menten data; Supplementary Figure 1C-E); similarly, the experimentally determined tRNase Z concentrations enter into the calculation of k_{cat} from V_{max} (Supplementary Table 1). Values used for substrate and enzyme concentrations were refined using analytical RNA and protein lanes by comparing dilutions from each experiment with standards. ΔFA and L187A display strikingly higher K_Ms than wild type tRNase Z with relatively small reductions in k_{cat} (Supplementary Figure 1D, E; cf C). Kinetic parameters from this experiments were combined with three others to obtain the mean ± standard errors presented in Supplementary Table 1 and the (variant relative to wild type) values on the bar graphs in Figure 2.

Supplementary Figure 1. **Processing kinetics with wild type, ΔFA and L187A tRNase Z^L**. A) Baculovirus expressed, affinity purified wild type, ΔFA183/226 and L187A tRNase Z^Ls were analyzed on a protein gel. 500 ng protein loads were detected by staining with Sypro orange (Molecular Probes) and scanned with a Typhoon 9420 (GE Healthcare). M: Invitrogen protein MW standards. Designations at left are marker protein sizes (kD). As expected for a 42 residue deletion, the MWApp for ΔFA is~5 kD lower than for WT and L187A tRNase Z. B) The canonical *D. melanogaster* $tRNA^{Arg}$ pre-tRNA substrate has a 17 nt 3' end trailer. → designates the tRNase Z cleavage site following the discriminator. (C) – (E) Michaelis-Menten experiments using constant input 5' end labeled substrate and varying concentrations of unlabelled substrate (designations at bottom, nM) with WT, ΔFA and L187A tRNase Z, respectively. Reactions were sampled after 5, 10 and 15 min. reaction at 28 C. Designations at right: substrate and product. Designations across top: 0 - a no processing control; enzyme (WT or variant) and concentration used. ~100-fold difference in enzyme concentration (e.g. 63 pM WT and 6.6 nM ΔFA) was based on results of efficiency experiments (not shown). The [S] ranges (5 - 125 nM for WT; 250 - 6250 nM for ΔFA and L187A) were based on repeated kinetic experiments in which the variants displayed a K_M one to two orders higher than WT tRNase Z. Michaelis-Menten plot with the kinetic parameters obtained by nonlinear regression analysis (SigmaPlot 11).

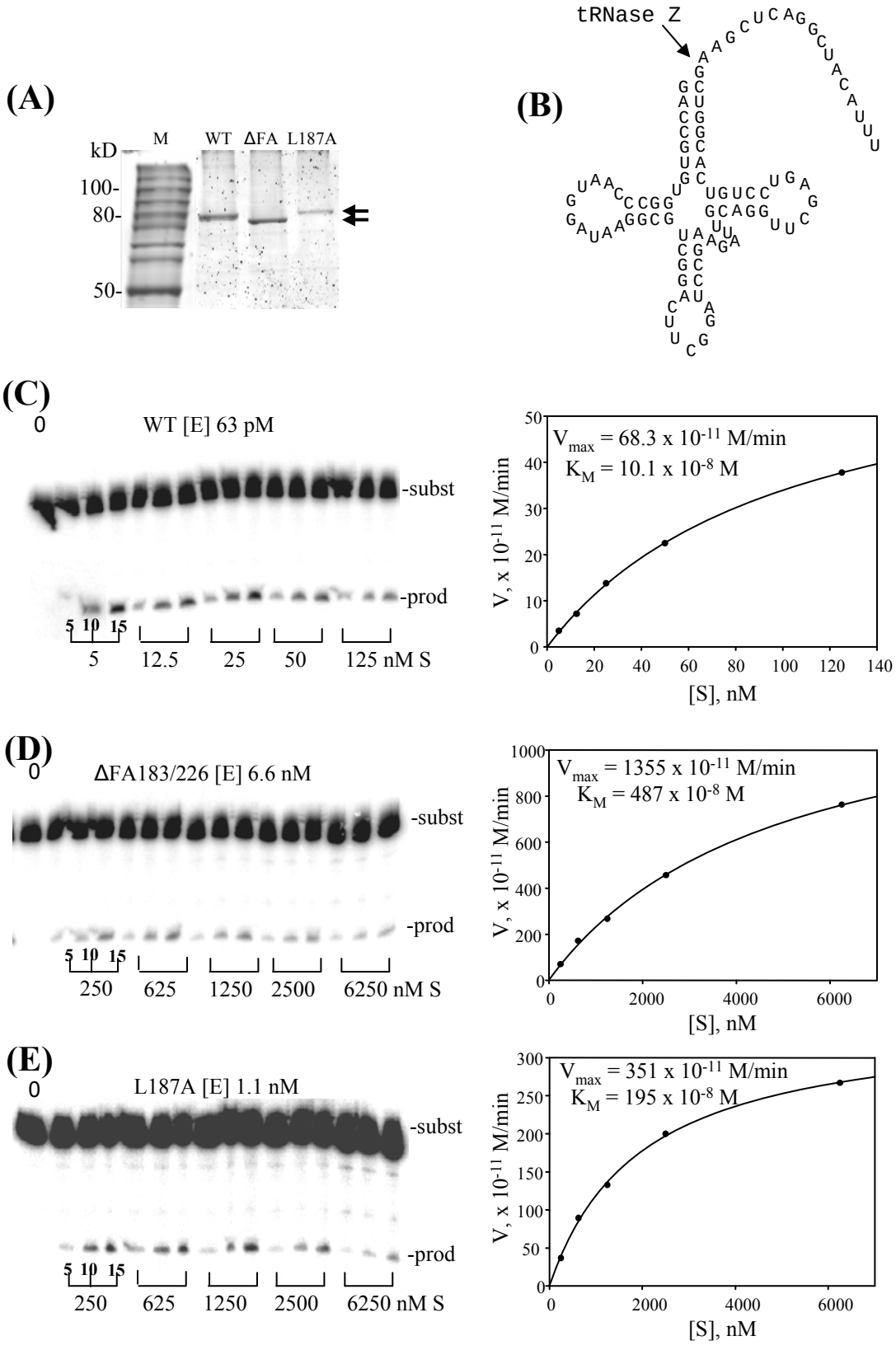

Levinger et al., 2009
Supplementary Figure 1

TABLE 1
Kinetic Parameters for Changes in the FA of *D. melanogaster* tRNase Z

tRNase Z	2° Struc	k_{cat} (min^{-1})	K_M (nM)	k_{cat}/K_M (X 10^8 $M^{-1}min^{-1}$)	Relative k_{cat}	Relative K_M	Relative k_{cat}/K_M
WT		7.8±1.2	34±4	2.7±0.2			
ΔFA		2.4±0.7	2820±680	0.012±0.006	0.31±0.11	76±12	0.0046±0.0006
G185	Asc St	1.9±0.5	12±4	1.6±0.3	0.64±0.25	1.0±0.4	0.83±0.27
A186T	Asc St	2.7±0.6	14±4	2.3±0.5	0.99±0.35	0.96±0.21	1.0±0.3
L187	St/α4	6.0±0.9	1380±340	0.056±0.018	0.86±0.22	64±24	0.017±0.004
N188	α4	1.1±0.2	21±4	0.53±0.08	0.34±0.14	1.8±0.04	0.19±0.08
L189	α4	0.78±0.11	9.7±1.0	0.82±0.11	0.34±0.11	0.84±0.07	0.41±0.14
V190	α4	1.9±0.4	33±3	0.60±0.17	0.28±0.02	1.1±0.09	0.24±0.00
K191	α4	5.7±0.8	15±3	4.1±1.3	2.4±0.7	3.5±1.7	0.7±0.07
C192	α4	8.7±3.1	37±11	2.7±0.5	1.4±0.5	1.4±0.2	1.1±0.4
V193	α4	7.2±2.1	52±15	1.5±0.5	1.1±0.4	2.5±0.6	0.5±0.2
E194	α4	1.0±0.2	18±2	0.58±0.06	0.51±.09	0.66±.16	0.79±.05
Q195	α4	2.8±0.7	19±4	1.4±0.5	0.50±0.18	1.4±0.6	0.39±0.13
G196	GP Loop	6.8±2.6	79±0.8	0.87±0.33	0.63±0.14	6.0±0.2	0.11±0.02
V197	GP Loop	2.3±0.7	590±170	0.44±0.13	0.40±0.18	5.0±1.8	0.077±0.007
P198	GP Loop	14±2	150±10	0.91±0.04	1.2±0.1	3.5±0.8	0.36±0.12
P199	GP Loop	22±5	140±30	1.6±0.13	2.6±1.1	4.0±1.4	0.68±0.17
G200	GP Loop	0.97±0.33	390±130	0.023±0.005	0.12±0.05	14±4	0.009±0.2
P201	GP Loop	46±13	280±60	1.7±0.3	3.1±0.2	4.9±1.4	0.70±0.18
L202	α5	12±0.5	130±30	1.0±0.2	0.43±0.09	1.4±0.4	0.32±0.02
L203	α5	0.84±0.08	44±7	0.20±0.05	0.37±0.06	4.2±0.4	0.088±0.004
G204	α5	1.2±0.1	40±14	0.33±0.09	0.74±0.26	3.1±1.4	0.25±0.03
Q205	α5	0.67±0.22	10±0. 9	0.69±0.28	0.37±0.02	0.78±0.16	0.50±0.14
L206	α5	0.24±0.08	140±20	0.017±0.003	0.13±0.01	11±0.3	0.013±0.0006
K207	α5	0.41±0.03	39±7	0.11±0.02	0.076±0.02	3.5±0.8	0.024±0.01
N208	α5	1.2±0.3	13±0. 5	0.94±0.21	0.41±0.07	0.80±0.17	0.51±0.02
G209	α5	0.38±0.16	49±10	0.074±0.017	0.21±0.003	4.1±1.1	0.054±0.014
N210	Loop	4.5±1.6	37±12	1.3±0.3	0.62±0.18	0.89±0.24	0.77±0.22
D211	Loop	6.0±2.3	180±70	0.34±0.09	0.40±0.14	3.1±0.3	0.13±0.04
I212	β10	2.5±0.7	120±40	0.30±0.14	0.35±0.11	4.1±1.3	0.09±0.03
T213	β10	1.1±0.01	19±2	0.56±0.07	0.28±0.005	1.1±0.4	0.29±0.10
L214	β10	0.43±0.15	47±5	0.10±0.03	0.17±0.07	3.3±0.7	0.049±0.012
P215	Loop	0.49±0.15	14±0. 6	0.36±0.13	0.14±0.05	1.0±0.01	0.14±0.05
D216	Loop	0.61±0.21	23±0. 1	0.26±0.08	0.15±0.05	1.7±0.08	0.086±0.028
G217	β11	0.54±0.11	32±0. 4	0.17±0.04	0.14±0.04	2.3±0.1	0.061±0.015
K218	β11	0.44±0.14	18±2.2	0.25±0.09	0.14±0.05	1.0±0.2	0.13±0.04
V219	β11	1.0±0.1	27±3	0.38±0.003	0.28±0.02	2.0±0.001	0.14±0.01
V220	Loop	4.1±1.5	35±16	1.6±0.5	0.38±0.04	0.62±0.03	0.75±0.15
R221	H	2.2±0.8	41±9	0.50±0.12	0.22±0.05	1.00±0.14	0.25±0.07
S222	H	1.9±0.9	31±6	0.61±0.27	0.93±0.08	2.9±0.5	0.37±0.07
V223	H	2.3±1.0	37±16	0.76±0.27	0.77±0.33	1.7±0.6	0.43±0.08
D224	Desc St	2.5±1.7	46±15	0.58±0.31	0.79±0.40	3.0±0.5	0.26±0.09

Table 1 column designations from left: wild type or variant tRNase Z, the wild type enzyme, deletion of the hand of the flexible arm (ΔFA 183/226) and the 40 residues substituted with Ala (G185 - D224 except that A186 was substituted with Thr). 2^o structure: designations are based on alignments (Figure 1A) and the structure of the *Bsu* tRNase Z^S B subunit (Figure 1B, C; 15; PDB #1Y44). k_{cat}, K_M, k_{cat}/K_M: values were obtained as in Supplementary Figure 1. Values reported are means of repeated experiments; variant processing experiments were performed at least twice and in most cases n = 3-4. Values following ± are standard errors. Three columns at right are k_{cat}, K_M and k_{cat}/K_M relative to WT (e.g. the quotient [k_{cat} variant]/[k_{cat} WT]). A wild type processing experiment was performed in parallel the same day as each variant processing experiment to control for day-to-day variations. Reported variant relative to WT values are the means and standard errors for specific experiments, and therefore differ from results that would be obtained by comparing values in columns to the left with aggregate means for WT (first row). Colored residues and values denote significant increases in K_M (blue) and reductions in k_{cat} (red).

Levinger et al., 2009, Supplementary Figure 2

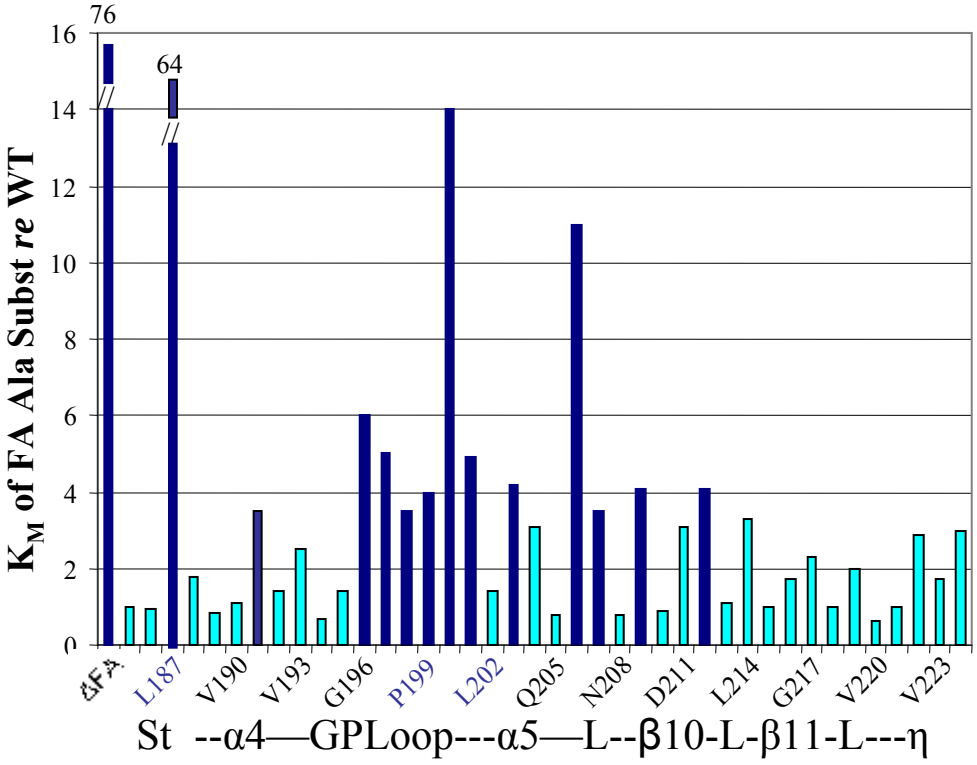

K_M of Ala substitutions relative to WT with ΔFA and L187A values suppressed to emphasize the K_M effects of the internal substitutions. The K_M relative to WT data from Table 1 as shown in Figure 2B except that // signifies the break in the data presented for ΔFA and L187A (76 and 64, respectively). The internal hand substitutions which lead to moderate increases in K_M (between 3.5 – 14-fold; dark blue) are clustered in the GP Loop (G196 – P201) and sprinkled at L206, K207, G209 and I212.

Levinger et al., 2009 Supplementary Figure 3

Presence of a bulky hydrophobic residue at the FA ascending stalk/hand boundary suggests that substitution at that position (L187A) could locally increase the flexibility of the hand, allowing it to fold over against the body of tRNase Z, which would establish a new stable contact (arrows in Supplementary Figure 3A), largely preventing the FA from binding substrate tRNA. Alternatively, a large decrease in net hydrophobicity and van der Waal's attractions in the interior of the FA hand (Supplementary Figure 3C, cf B) could allow collapse of the globular FA hand arising from the L187A substitution. Because hypothesized structural changes caused by the L187A substitution would occur in the absence of substrate, they can be effectively modeled using the protein-only structure (15).

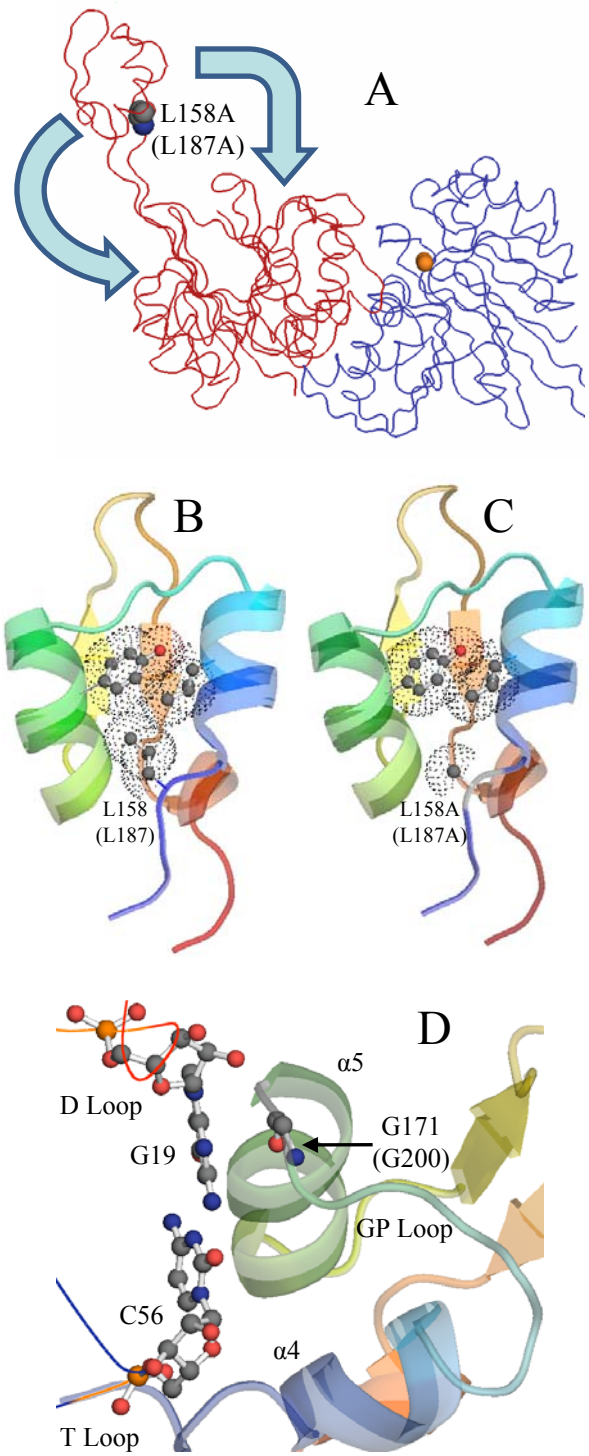

Supplementary Figure 3. **Interpretive views of the FA free and in a complex with tRNA**. A) *B. subtilis* L158 (L187 in *Dme* tRNase Z) and possible effects of the L187A substitution on tRNase Z structure (from 15; PDB# 1Y44). Curved arrows indicate repositioning of the FA that would arise from hypothesized increased flexibility at the ascending stalk/hand boundary and a new interaction between the FA hand and the body of tRNase Z. L158 is displayed with space-filling and the rest of tRNase Z in ribbon. (B), (C) Modeled density of van der Waal's repulsions with WT and L187A tRNase Zs, respectively. Backbone of the FA hand is displayed in cartoon, bulky hydrophobic R-groups are displayed in ball-and-stick and van der Waal's contacts are modeled with dots. (B) is the wild type and (C) is the L158A substitution (L187A in *D. melanogaster* tRNase Z). D) G170 (G200 in *Dme* tRNase Z). The backbone in this part of the GP loop (from 20; PDB# 2FK6) is within contact distance of the G19-C56 tertiary base pair in the tRNA.

The GP loop in the vicinity of G200 runs parallel to the axis of the G19/C56 base pair, within contact distance for a favorable stacking interaction (Supplementary Figure 3D).

Levinger et al., 2009 Supplementary Figure 3